Time-Domain Representations of a Plane Wave with Spatial Band-Limitation in the Spherical Harmonics Domain

Nara Hahn and Sascha Spors
Institute of Communications Engineering
University of Rostock, Germany
nara.hahn@uni-rostock.de

Introduction

Spherical harmonics expansion is often used to describe the sound field captured by a microphone array or the target sound field to be reproduced by a loudspeaker array [1–4]. The majority of the related signal processing methods are formulated in the temporal frequency domain which require a substantial amount of computation due to the involved spherical Bessel and Hankel functions. As demonstrated in a number of studies, time-domain implementations can reduce the computational complexity considerably [5–8]. Therefore, it is of interest to describe a spherical harmonics expansion in the time domain. In this paper, the time-domain representation for a plane wave is derived based on (a) inverse Fourier transform (b) Laplace domain representation and (c) plane wave expansion, all of which are mathematically equivalent in the continuous time domain. Based on these representations, the spatio-temporal properties of the sound field are investigated.

Nomenclature A position vector is denoted by lowercase boldface $\boldsymbol{x} = (r, \theta, \phi)$, where $r = \|\boldsymbol{x}\|$ denotes the radius, θ the colatitude, and ϕ the azimuth. The unit vector in the same direction is denoted by $\hat{\boldsymbol{x}} = \frac{\boldsymbol{x}}{r} = (1, \theta, \phi)$. The scalar product of two vectors, $\boldsymbol{x}$ and $\boldsymbol{y}$, is denoted by $\langle \boldsymbol{x}, \boldsymbol{y} \rangle$. The angular frequency is denoted by $\omega = 2\pi f$ with f being the temporal frequency. The imaginary unit is denoted by i, and the speed of sound by c. The asterisk in the superscript $(\cdot)^*$ denotes the complex conjugate. The Fourier and Laplace transforms are denoted by $\mathcal{F}\{\cdot\}$ and $\mathcal{L}\{\cdot\}$, respectively, whereas their inverse transforms by the superscript $(\cdot)^{-1}$.

Spherical Harmonics Expansion

The sound field of a plane wave propagating in the direction $\boldsymbol{n}_{\mathrm{pw}} = (1, \theta_{\mathrm{pw}}, \phi_{\mathrm{pw}})$ can be expanded in terms of spherical harmonics as [2, Ch. (2.37)]

$$\begin{aligned} & e^{-i\frac{\omega}{c} r \langle \boldsymbol{n}_{\mathrm{pw}}, \hat{\boldsymbol{x}} \rangle} \\ &= \sum_{n=0}^{\infty} \sum_{m=-n}^{n} 4\pi i^{-n} j_n(\tfrac{\omega}{c} r) Y_{nm}^*(\boldsymbol{n}_{\mathrm{pw}}) Y_{nm}(\hat{\boldsymbol{x}}) \\ &= \sum_{n=0}^{\infty} (2n+1) i^{-n} j_n(\tfrac{\omega}{c} r) P_n\big(\langle \boldsymbol{n}_{\mathrm{pw}}, \hat{\boldsymbol{x}} \rangle\big), \end{aligned} \tag{1}$$

where $Y_{nm}(\cdot)$ denotes the spherical harmonic of order n and degree m, $j_n(\cdot)$ the spherical Bessel function of the first kind, and $P_n(\cdot)$ the Legendre function. In the second equality, the addition theorem of the Legendre function is exploited [9, Eq. (14.18.2)]. The time dependent term $e^{i\omega t}$ is omitted.

A spherical harmonics expansion is called spatially band-limited, if the infinite summation (1) is truncated up to a finite order N, i.e. $n = 0, 1, \ldots, N$ and $m = -n, \ldots, n$. The maximum order N is defined as the spatial bandwidth. A spatially band-limited expansion is still a reasonable approximation of the sound field within a sphere $r < \frac{cN}{\omega}$ centered at the origin [2, Sec. 2.3].

Inverse Fourier Transform

The time-domain representation of (1) can be obtained by exploiting the inverse Fourier transform of $j_n(\frac{\omega}{c} r)$ [9, Eq. (10.59.1)],

$$\begin{aligned} \mathcal{F}^{-1}\{j_n(\tfrac{\omega}{c} r)\} &= \frac{i^n c}{2r} \tilde{P}_n(\tfrac{c}{r} t) \\ &= \frac{i^n c}{2r} \cdot \begin{cases} P_n(\frac{c}{r} t), & |t| < \frac{r}{c} \\ \frac{1}{2}(\pm 1)^n, & t = \pm \frac{r}{c} \\ 0, & |t| > \frac{r}{c}. \end{cases} \end{aligned} \tag{2}$$

The inverse Fourier transform of a spatially band-limited plane wave thus reads

$$q(\boldsymbol{x}, t) = \frac{c}{2r} \sum_{n=0}^{N} (2n+1)\, \tilde{P}_n(\tfrac{c}{r} t)\, P_n\big(\langle \boldsymbol{n}_{\mathrm{pw}}, \hat{\boldsymbol{x}} \rangle\big), \tag{3}$$

which constitutes a series representation of the Dirac delta function $\delta\big(t - \frac{r}{c}\langle \boldsymbol{n}_{\mathrm{pw}}, \hat{\boldsymbol{x}} \rangle\big)$ for $N \to \infty$ [10, Eq. (1.8)] [11, Sec. 1.3]. Note from (2) that the time-domain signal has a finite support within $|t| \leq \frac{r}{c}$.

In Fig. 1(a), a spatially band-limited ($N = 10$) plane wave is shown for different time instants $t \leq 0$. A spherical wavefront with radius $r = |ct|$ shrinks toward the origin and vanishes at $t = 0$. The wavefront ⋯ of the original plane wave ($N \to \infty$) is spatially spread and exhibits a bow-tie-like shape ⋈. This component gets thinner for higher spatial bandwidths. The sound fields for $t < 0$ and $t > 0$ are symmetric with respect to the x-axis. For $t > 0$ (not shown here), the wavefront ⋈ propagates further in the $-y$ direction, and the spherical wavefront expands from the origin. Similar observations are found in [4, Sec. 2.2.2], where the time-domain sound field is obtained numerically by inverse discrete Fourier transform of (1).

Figure 1(b) shows the impulse responses at different positions. The response at 'Center' resembles a Dirac-shaped

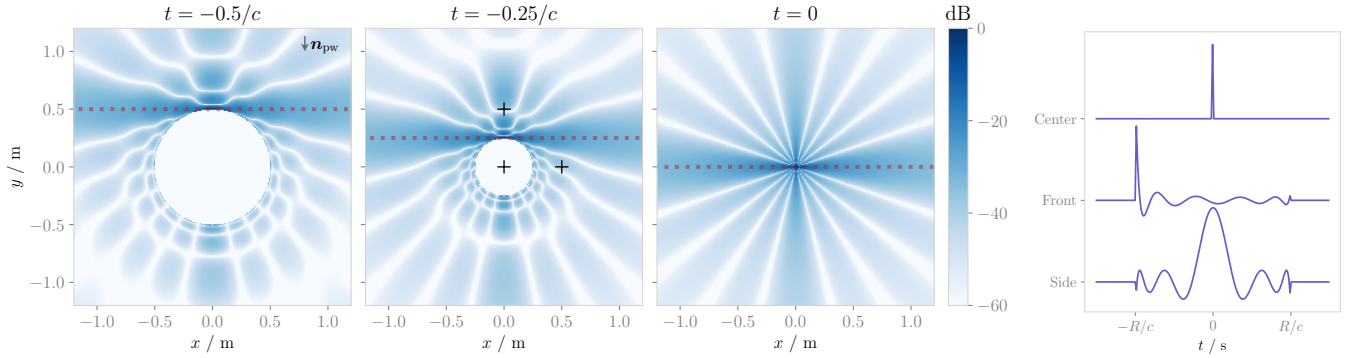

(a) (b)

Figure 1: (a) Sound field of a plane wave propagating in the $-y$ direction with a spatial bandwidth of $N = 10$. The logarithmic amplitudes (dB scale) are shown for different time instants. The dotted lines ··· indicate the wavefront of the original plane wave ($N \to \infty$). (b) Impulse responses at different positions, 'Center' $(0, 0, 0)$, 'Front' $(0, R, 0)$, and 'Side' $(R, 0, 0)$ with $R = 0.5$ m, indicated by '+' in (a). The peaks are normalized for ease of comparison.

impulse, whereas at off-center positions with $R = 0.5$, the signals are temporally spread within $|t| \leq \frac{R}{c}$. The response at 'Side' exhibits a sinc-shaped waveform indicating a low-pass filtered characteristic. The spectral distortion at 'Front' is less severe due to the dominant peak around $t = -\frac{R}{c}$. The influence of a spatial band-limitation therefore depends on the angular difference $\cos^{-1}\left(\langle \boldsymbol{n}_{\mathrm{pw}}, \hat{\boldsymbol{x}} \rangle\right)$ as well as on the distance from the expansion center. This agrees with the observations in [4, Sec. 2.2.2].

For a discrete-time modelling, (3) has to be sampled uniformly in the time domain. Aliasing is inevitable in this process as $j_n(\cdot)$ is not band-limited in the ω-domain. Considering the large argument approximation $j_n(z) \approx \frac{1}{z} \sin\left(z - \frac{n\pi}{2}\right)$ [12, Eq. (11.158)], the aliasing energy can be reduced to some extent by oversampling.

Laplace Domain

In this section, the frequency domain representation (1) is converted into a system function by substituting the temporal frequency with a complex variable in the Laplace domain. The spherical Bessel function then reads [9, Eq. (10.47.10)]

$$j_n(\tfrac{\omega}{c} r) \to j_n(s) = \frac{1}{2}\Big[\underbrace{-i^{-n} e^{+s} \sum_{k=0}^{n} \alpha_n(k)\, (-s)^{-k-1}}_{h_n^{(1)}(s)} \underbrace{-i^{+n} e^{-s} \sum_{k=0}^{n} \alpha_n(k)\, s^{-k-1}}_{h_n^{(2)}(s)} \Big], \quad (4)$$

where $h_n^{\{(1),(2)\}}(s) = j_n(s) \pm i y_n(s)$ denotes the spherical Hankel function of the first and second kind ($y_n(s)$: spherical Neumann function). The series expansions of the spherical Hankel functions [9, Eq. (10.49.6) and (10.49.7)] are exploited which are described by the coefficients $\alpha_n(k) = \frac{(n+k)!}{(n-k)!k!2^k}$ [9, Eq. (10.49.1)].

Since each expansion exhibits $n + 1$ poles at $s = 0$, the region of convergence (ROC) is either $\Re\{s\} > 0$ or $\Re\{s\} < 0$, meaning that the Fourier transform does not converge [13, Sec. 9.2]. However, the instabilities of the individual systems disappear once the system functions are combined, as shown in the following derivation. This is indeed expected from (2) as the time-domain signal is of finite duration and absolutely integrable, for which the Fourier transform should exist [13, Sec. 9.2].

Let us assume that $\Re\{s\} > 0$. Since [13, Sec. 9.6]

$$\mathcal{L}^{-1}\left\{\frac{e^{-\tau s}}{s^{n+1}}\right\} = \frac{1}{n!}(t-\tau)^n\, u(t-\tau), \quad (5)$$

the inverse Laplace transform of (4) reads

$$\mathcal{L}^{-1}\{j_n(s)\} = \frac{1}{2}\Big[i^{-n} u(t+1) \sum_{k=0}^{n} \frac{\alpha_n(k)}{k!} (-t-1)^k - i^{+n} u(t-1) \sum_{k=0}^{n} \frac{\alpha_n(k)}{k!} (t-1)^k \Big], \quad (6)$$

for ROC $\supseteq \Re\{s\} > 0$, where $u(t)$ denotes the unit step function defined as

$$u(t) = \begin{cases} 0, & \text{for } t < 0 \\ \frac{1}{2}, & \text{for } t = 0 \\ 1, & \text{for } t > 0. \end{cases} \quad (7)$$

The time-domain signal thus consists of two right-sided signals, one with a negative delay and the other with a positive delay. By exploiting

$$\frac{\alpha_n(k)}{k!} = \frac{(n+k)!}{(n-k)!k!2^k k!} = \binom{n}{k}\binom{n+k}{k}\frac{1}{2^k} \quad (8)$$

and [14, Eq. (0.1)]

$$P_n(\pm t) = \sum_{k=0}^{n} \binom{n}{k}\binom{n+k}{k}\left(\frac{\pm t - 1}{2}\right)^k, \quad (9)$$

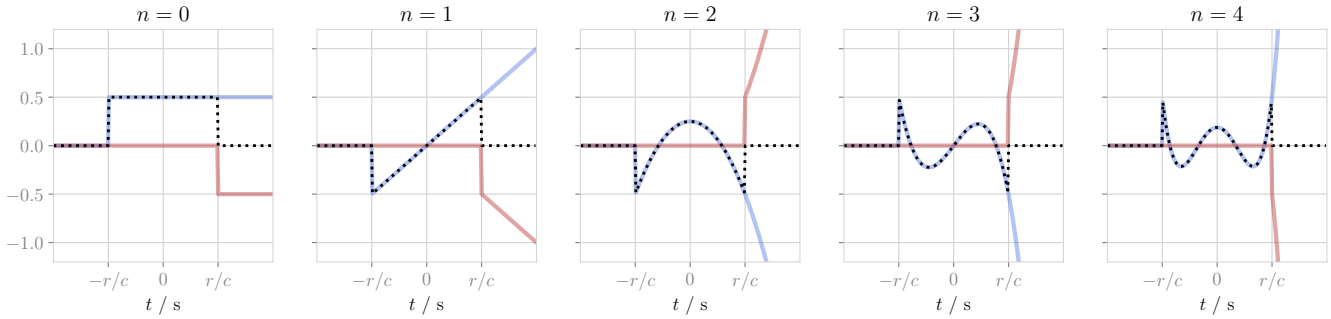

Figure 2: Time-domain signals constituting the inverse Laplace transforms, $\mathcal{L}^{-1}\{\frac{1}{2}h_n^{(1)}(\frac{s}{c}r)\}$ — and $\mathcal{L}^{-1}\{\frac{1}{2}h_n^{(2)}(\frac{s}{c}r)\}$ —, for $\Re\{s\} > 0$ and $n = 0, 1, \ldots, 4$, cf. (6). The diverging components for $t > \frac{r}{c}$ cancel each other, and the remaining part ⋯ constitutes the inverse Laplace transform $\mathcal{L}^{-1}\{j_n(\frac{s}{c}r)\}$, cf. (10). The real parts are plotted for even n, and the imaginary parts for odd n.

where $\binom{\cdot}{\cdot}$ denotes the binomial coefficient, (6) reads

$$\begin{aligned}\mathcal{L}^{-1}\{j_n(s)\} &= \frac{1}{2}\Big[i^{-n}u(t+1)P_n(-t) - i^n u(t-1)P_n(t)\Big] \\ &= \frac{i^n}{2}P_n(t)\big[u(t+1) - u(t-1)\big] \\ &= \frac{i^n}{2}\tilde{P}_n(t). \end{aligned} \tag{10}$$

The anti-symmetry $P_n(-t) = (-1)^n P_n(t)$ is used in the second equality. Although not shown here, the inverse Laplace transform for $\Re\{s\} < 0$ gives the same result. Finally, the inverse Fourier transform is evaluated by substituting $s \to i\frac{\omega}{c}r$ $(t \to \frac{c}{r}t)$,

$$\mathcal{F}^{-1}\{j_n(\tfrac{\omega}{c}r)\} = i^n \frac{c}{2r}\tilde{P}_n(\tfrac{c}{r}t), \tag{11}$$

which leads to the same expression as (2).

From a system theoretical perspective, the time-domain signal $\mathcal{L}^{-1}\{j_n(\frac{s}{c}r)\}$ or $\mathcal{F}^{-1}\{j_n(\frac{\omega}{c}r)\}$ can be modelled as a parallel connection of two recursive filters. The filter parameters (e.g. poles and zeros) can be obtained by analyzing the system functions given by (4). Although the impulse responses of the individual filters are infinitely long and diverging, the combined impulse response is of finite duration. This is shown in Fig. 2 where $\mathcal{L}^{-1}\{\frac{1}{2}h_n^{(1)}(\frac{s}{c}r)\}$ — and $\mathcal{L}^{-1}\{\frac{1}{2}h_n^{(2)}(\frac{s}{c}r)\}$ — exactly cancel each other for $t > \frac{r}{c}$ and add up to $\frac{i^n}{2}\tilde{P}_n(\frac{c}{r}t)$ ⋯.

In practice, however, even a slight time misalignment of the filters or quantization errors can cause an imperfect cancellation, thereby resulting in a diverging impulse response [15, Ch. 4]. As a workaround, a finite impulse response (FIR) filter can be designed by windowing the output of the recursive filter. In this case, only the first filter $\mathcal{L}^{-1}\{h_n^{(1)}(\frac{s}{c}r)\}$ is needed which fully describes the response for $|t| \leq \frac{r}{c}$.

Plane Wave Expansion

In a plane wave expansion (PWE), a sound field is represented as a superposition of plane waves [2, Eq. (2.42)],

$$Q(\boldsymbol{x},\omega) = \int_{\partial\Omega} \bar{Q}(\boldsymbol{n}) e^{-i\frac{\omega}{c}r\langle \boldsymbol{n},\hat{\boldsymbol{x}}\rangle} \mathrm{d}A(\boldsymbol{n}) \tag{12}$$

where $\boldsymbol{n} = (1, \tilde{\theta}, \tilde{\phi})$ denotes the direction of each plane wave and $\bar{Q}(\boldsymbol{n})$ the corresponding coefficient. The surface integral on the unit sphere is denoted by $\int_{\partial\Omega}\mathrm{d}A(\boldsymbol{n}) = \int_0^{\pi}\int_0^{2\pi}\sin\tilde{\theta}\,\mathrm{d}\tilde{\phi}\,\mathrm{d}\tilde{\theta}$. The PWE coefficient for a spatially band-limited plane wave reads [2, Eq. (2.43)]

$$\bar{Q}(\boldsymbol{n}) = \sum_{n=0}^{N}\sum_{m=-n}^{n} Y_{nm}^*(\boldsymbol{n}_{\mathrm{pw}})Y_{nm}(\boldsymbol{n}) \tag{13}$$

$$= \sum_{n=0}^{N} \tfrac{2n+1}{4\pi} P_n(\langle \boldsymbol{n}_{\mathrm{pw}}, \boldsymbol{n}\rangle), \tag{14}$$

which constitutes a 2-dimensional Dirac delta function $\delta(\cos\tilde{\theta} - \cos\theta_{\mathrm{pw}})\delta(\tilde{\phi} - \phi_{\mathrm{pw}})$ for $N \to \infty$ [12, p. 792].

Since the PWE coefficient (14) is independent of ω, and thus $\mathcal{F}^{-1}\{\bar{Q}(\boldsymbol{n})\} = \bar{Q}(\boldsymbol{n})\cdot\delta(t)$, the inverse Fourier transform of (12) is

$$\begin{aligned} q(\boldsymbol{x},t) &= \int_{\partial\Omega} \mathcal{F}^{-1}\{\bar{Q}(\boldsymbol{n})\} *_t \delta\big(t - \tfrac{r}{c}\langle \boldsymbol{n},\hat{\boldsymbol{x}}\rangle\big)\mathrm{d}A(\boldsymbol{n}) \\ &= \int_{\partial\Omega} \bar{Q}(\boldsymbol{n})\ \delta\big(t - \tfrac{r}{c}\langle \boldsymbol{n},\hat{\boldsymbol{x}}\rangle\big)\mathrm{d}A(\boldsymbol{n}), \end{aligned} \tag{15}$$

where $*_t$ denotes the convolution in the time domain. The plane waves arriving at $\boldsymbol{x}$ for a given time $t \in [-\frac{r}{c}, \frac{r}{c}]$ exhibit the axis-symmetry $t = \frac{r}{c}\langle \boldsymbol{n},\hat{\boldsymbol{x}}\rangle$. For $|t| > \frac{r}{c}$, the integral (15) is zero and no plane wave arrives. This explains the finite extent of the time-domain signal (3).

The direction- and time-of-arrival of the individual plane waves are depicted in Fig. 3. Notice that the plane wave amplitude is determined by $\langle \boldsymbol{n}_{\mathrm{pw}}, \boldsymbol{n}\rangle$, whereas the time-of-arrival by the receiver position $\boldsymbol{x}$. At 'Center', all plane waves arrive simultaneously at $t = 0$, resulting in a Dirac-shaped impulse. At off-center positions, the time-of-arrival is distributed in $t \in [-\frac{r}{c}, \frac{r}{c}]$. At 'Front', the plane wave direction changes gradually from $-y$ to $+y$, whereas at 'Side', it changes from $-x$ to $+x$. It is clear at this point that the spherical wavefront observed in Fig. 1(a) is formed by the superimposed planar wavefronts all of which are at the same distance $|ct|$ from the origin.

The equivalence of the time-domain PWE (15) and the

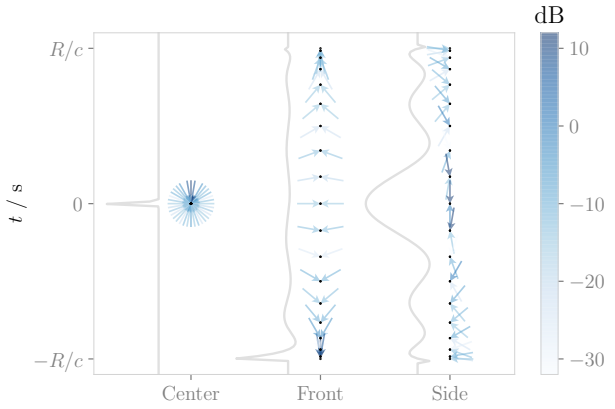

Figure 3: Plane wave direction and time-of-arrival (same parameters as in Fig. 1). The plane wave directions are indicated by arrows, whose tips are pointing at the corresponding time-of-arrival indicated by dots ·. Only the plane waves in the xy-plane, i.e. $\boldsymbol{n} = (1, \frac{\pi}{2}, \tilde{\phi})$, are shown for better visualization. The color map indicates the logarithmic amplitude of the individual plane waves. The gray curves are the corresponding impulse responses from Fig. 1(b).

spherical harmonics expansion (3) can be shown by plugging (13) into (15),

$$
\begin{aligned}
&q(\boldsymbol{x}, t) \\
&= \sum_{n=0}^{N} \sum_{m=-n}^{n} Y_{nm}^{*}(\boldsymbol{n}_{\mathrm{pw}}) \int_{\partial\Omega} \delta\left(t - \tfrac{r}{c}\langle \boldsymbol{n}, \hat{\boldsymbol{x}} \rangle\right) Y_{nm}(\boldsymbol{n}) \, \mathrm{d}A(\boldsymbol{n}) \\
&= 2\pi \sum_{n=0}^{N} \sum_{m=-n}^{n} Y_{nm}^{*}(\boldsymbol{n}_{\mathrm{pw}}) Y_{nm}(\hat{\boldsymbol{x}}) \int_{-1}^{1} \delta(t - \tfrac{r}{c}\mu) \, P_n(\mu) \, \mathrm{d}\mu \\
&= \frac{c}{2r} \sum_{n=0}^{N} (2n+1) P_n(\langle \boldsymbol{n}_{\mathrm{pw}}, \hat{\boldsymbol{x}} \rangle) \tilde{P}_n(\tfrac{c}{r} t),
\end{aligned} \tag{16}
$$

where the Funk-Hecke theorem [1, Sec. 2.1.2][16, Eq. (8)],

$$
\begin{aligned}
&\int_{\partial\Omega} f(\langle \boldsymbol{n}_1, \boldsymbol{n}_2 \rangle) \, Y_{nm}(\boldsymbol{n}_1) \, \mathrm{d}A(\boldsymbol{n}_1) \\
&\qquad = 2\pi Y_{nm}(\boldsymbol{n}_2) \int_{-1}^{1} f(\mu) \, P_n(\mu) \, \mathrm{d}\mu,
\end{aligned} \tag{17}
$$

is exploited in the second equality.

In practice, (15) has to be sampled in space and time. A finite number of plane waves has to be chosen by taking the spatial bandwidth into account, so that the integral is adequately approximated [17]. The time delays must be realized with fractional delay filters for a reasonable temporal resolution [18].

Conclusion

In this paper, a time-domain representation of the spherical harmonics expansion is introduced for a plane wave. The representation is obtained via inverse Fourier transform, inverse Laplace transform, and plane wave expansion. Each derivation reveals distinct aspects of the sound field. For practical usage, the representations should be discretized in time and/or space, which then leads to different discrete-time models. These can be used for time-domain implementations of signal processing techniques that are based on spherical harmonics expansion. Compared to frequency-domain implementation, the computational efficiency is expected to be improved as the evaluation of spherical Bessel function is not required.

References

[1] N. A. Gumerov and R. Duraiswami, *Fast Multipole Methods for the Helmholtz Equation in Three Dimensions*. Elsevier, 2005.

[2] B. Rafaely, *Fundamentals of Spherical Array Processing*. Springer, 2015.

[3] J. Daniel, "Représentation de champs acoustiques, application à la transmission et à la reproduction de scènes sonores complexes dans un contexte multimédia," Ph.D. dissertation, University of Paris VI, 2001.

[4] J. Ahrens, *Analytic Methods of Sound Field Synthesis*. Springer, 2012.

[5] H. Pomberger, "Angular and Radial Directivity Control for Spherical Loudspeaker Arrays," Diploma Thesis, University of Music and Performing Arts, Graz, Austria, 2008.

[6] S. Spors, V. Kuscher, and J. Ahrens, "Efficient Realization of Model-based Rendering for 2.5-dimensional Near-field Compensated Higher Order Ambisonics," in *Proc. IEEE Workshop Appl. Signal Process. Audio Acoust. (WASPAA)*, New Paltz, USA, Oct. 2011.

[7] F. Winter, N. Hahn, and S. Spors, "Time-Domain Realisation of Model-Based Rendering for 2.5D Local Wave Field Synthesis Using Spatial Bandwidth-Limitation," in *Proc. Eur. Signal Process. Conf. (EUSIPCO)*, Kos, Greece, 2017.

[8] N. Hahn, F. Winter, and S. Spors, "Synthesis of a Spatially Band-Limited Plane Wave in the Time-Domain Using Wave Field Synthesis," in *Proc. Eur. Signal Process. Conf. (EUSIPCO)*, Kos, Greece, 2017.

[9] F. W. Olver, D. W. Lozier, R. F. Boisvert, and C. W. Clark, *NIST Handbook of Mathematical Functions Handback*. Cambridge University Press, 2010.

[10] Y. Li and R. Wong, "Integral and Series Representations of the Dirac Delta Function," *Commun. on Pure & Appl. Anal.*, vol. 7, no. 2, pp. 229–247, 2008.

[11] R. P. Kanwal, *Generalized Functions Theory and Technique: Theory and Technique*. Springer Science & Business Media, 2012.

[12] G. B. Arfken and H. J. Weber, *Mathematical Methods for Physicists*. Academic press, 2005.

[13] A. V. Oppenheim, A. S. Willsky, and S. H. Nawab, *Signals and Systems*, 1983.

[14] W. Koepf, *Hypergeometric Summation*. Springer, 1998.

[15] R. Baumgartner, "Time Domain Fast-Multipole Translation for Ambisonics," Diploma Thesis, University of Music and Performing Arts, Graz, Austria, 2011.

[16] E. Hecke, "Über orthogonal-invariante Integralgleichungen," *Mathematische Annalen*, vol. 78, no. 1, pp. 398–404, 1917.

[17] F. Zotter, "Sampling Strategies for Acoustic Holography/Holophony on the Sphere," in *Proc. German Annu. Conf. Acoust. (DAGA)*, Rotterdam, The Netherlands, 2009.

[18] T. I. Laakso, V. Valimaki, M. Karjalainen, and U. K. Laine, "Splitting the Unit Delay," *IEEE Signal Process. Mag.*, vol. 13, no. 1, pp. 30–60, 1996.